ON THE TIME SPLITTING SPECTRAL METHOD FOR THE COMPLEX GINZBURG–LANDAU EQUATION IN THE LARGE TIME AND SPACE SCALE LIMIT*

PIERRE DEGOND†, SHI JIN‡, AND MIN TANG§

Abstract. We are interested in the numerical approximation of the complex Ginzburg–Landau equation in the large time and space limit. There are two interesting regimes in this problem, one being the large space time limit, and one being the nonlinear Schrodinger limit. These limits have been studied analytically in, for example, [7, 18, 19]. We study a time splitting spectral method for this problem. In particular, we are interested in whether such a scheme is asymptotic preserving (AP) with respect to these two limits. Our results show that the scheme is AP for the first limit, but not the second one. For the large space time limit, our numerical experiments show that the scheme can capture the correct physical behavior without resolving the small scale dynamics, even for transitional problem where small and large scales coexist.

Key words. Asymptotic preserving scheme; complex Ginzburg–Landau equation; asymptotic limit; time splitting spectral method

AMS subject classifications. 35Q55,65M70

1. Introduction. The complex Ginzburg–Landau equation (CGL) is one of the most studied nonlinear equations in the physics history. It has a long history in physics as a generic amplitude equation near the onset of instabilities that lead to chaotic dynamics in fluid mechanical systems. The case with real coefficients was first derived by Newell and Whiteehead [25] and Segel [27] to describe Bénard convection. The case with complex coefficients was put forth in a general setting by Newell and Whitehead [24] and DiPrima et al. [11], and was shown by Stewartson and Stuart [28] to apply to plane Poiseuille flow. It also describes a vast variety of phenomena like phase transitions, superfluidity, superconductivity and Bose–Einstein condesation [9, 10].

The generalized scaled CGL can be written as

$$\partial_t u = u + (1 + i\nu)\triangle u - (1 + i\mu)|u|^2 u, \tag{1.1}$$

where u is a complex function of (scaled) time t and space $\vec{x}$. ν, μ are real parameters characterizing linear and nonlinear dispersion. The second spatial derivative provides a damping of the short wavelength excitations and the nonlinear term generates energy flows from large to short scales. To consider the large space and time scales, we rescale

* This work was completed during the stay of the second and third authors in the Institute of Mathematics of Toulouse.

†Institute of Mathematics of Toulouse UMR 5219 (CNRS-UPS-INSA-UT1-UT2), Université Paul Sabatier, 118, route de Narbonne, 31062 Toulouse cedex, France. The first author wishes to acknowledge the support from the french ANR under contract 'Quatrain' number BLAN07-2_212988.(degond@mip.ups-tlse.fr).

‡Department of Mathematics, University of Wisconsin, Madison, WI 53706, USA; Department of Mathematical Sciences, Tsinghua University, Beijing 100084, China. The second author acknowledges the support of NSF grant No. DMS-0608720. The second author was also supported by a grant from 'Centre National de la Recherche Scientifique'(jin@math.wisc.edu)

§Department of Mathematical Sciences, Tsinghua University, Beijing 100084, China. The third author was supported by the Marie Curie Actions of the European Commission in the frame of the DEASE project (MEST-CT-2005-021122) and NSFC project 10676017(tangmin@mails.tsinghua.edu.cn)

the original equation by

$$t' = \epsilon^2 t, \qquad x' = \epsilon x. \tag{1.2}$$

which gives (dropping the primes)

$$\partial_t u = (1 + i\nu)\triangle u + \frac{1}{\epsilon^2}\Big(u - (1 + i\mu)|u|^2 u\Big). \tag{1.3}$$

Using the change of unknown $u = e^{-i\mu t/\epsilon^2}\tilde{u}$ into the above equation gives

$$\partial_t \tilde{u} = (1 + i\nu)\triangle \tilde{u} + \frac{1}{\epsilon^2}(1 + i\mu)\big(1 - |\tilde{u}|^2\big)\tilde{u}.$$

When $\mu = \nu > 0$, let

$$\mu = \nu = \frac{1}{\delta},$$

and rescale time and space again by

$$t' = \frac{(\delta^2 + 1)}{\delta} t, \qquad x' = x\,, \tag{1.4}$$

then one gets a special form of the complex Ginzburg–Landau equation

$$\delta\partial_t u_\epsilon - i\partial_t u_\epsilon = \triangle u_\epsilon + \frac{1}{\epsilon^2}(1 - |u_\epsilon|^2)u_\epsilon, \quad x \in \Omega.$$

When $\mu = \nu < 0$, let

$$\mu = \nu = -\frac{1}{\delta},$$

and using the same rescaling as in (1.4), one gets

$$\delta\partial_t u_\epsilon + i\partial_t u_\epsilon = \triangle u_\epsilon + \frac{1}{\epsilon^2}(1 - |u_\epsilon|^2)u_\epsilon, \quad x \in \Omega\,. \tag{1.5}$$

When $\delta = 0$, that is, $\nu = \mu = \infty$, the equation becomes the nonlinear Schrödinger equation (NLS). Colin and Soyeur [7] and Lin and Xin [18, 19] studied the dynamic limit of the above equation when $\epsilon \to 0$. If there are vortices in the initial data, that is $|u_\epsilon(x_0)| = 0$, and the phase of u_ϵ has singularities at x_0 points, it is proved that the energy concentrates near the vortices as $\epsilon \to 0$. Thus the limit solution is not smooth. It can be proved that the limit equation is

$$\delta u_t - \triangle u = u|\nabla u|^2, \quad |u| = 1 \quad a.e., \quad u(0) = \psi. \tag{1.6}$$

We would like to study the performance of a time splitting spectral method (TSSP) for the CGL in the regime where $\epsilon << 1$ and $\delta << 1$. A TSSP is natural for a Schrödinger type equation (see for example [26]). It is very attractive in the semiclassical regime [4, 5]. Such a scheme was applied to the CGL to study its vortex dynamics in [2, 3] in the regime where $\epsilon = O(1), \delta = O(1)$. When $\epsilon << 1, \delta << 1$, whether these method is still adequate for the CGL, in terms of consistency, stability and converge, remains unknown. TSSP was extended to Zakharov equations [16] and the Dirac–Maxwell system [14] with good asymptotic preserving properties in various

regimes. In spite of extensive applications of time splitting spectral methods for both linear and nonlinear Schrödinger type equations, there has been no rigorous convergency study for these fully discrete methods. In this regard, we would like to mention error analysis on time splitting —by keeping the spatial variable continuous—methods for nonlinear Schrödinger equations [6, 22].

Other numerical methods, including nonsplitting spectral method [29], and finite difference methods [12, 20, 21], have been developed for the CGL. But their performance in the regimes of our interest has not been studied.

Asymptotic preserving (AP) methods are attractive for PDEs with small parameters, since they work for all range of the corresponding parameter. A scheme is AP if it possesses the discrete analogy of the continuous asymptotic limit as the small parameter goes to zero. More precisely, it is a good scheme for the original equation, and in the limit as the small parameter goes to zero, becomes a good scheme for the continuous limit equation [15]. Such a scheme could be convergent uniformly with respect to the small parameter (see [13]), thus correct (macroscopic) physical behavior, when the small parameter is small, can be captured even if the numerical computation is *underresolved* (the mesh size and time step much larger than the small space/time parameters). For a problem involving different scales, AP methods avoid the interface conditions used in most other multiscale methods to connect models of different scales.

In this paper, we give heuristic arguments about the AP property of the TSSP for the CGL (1.5). We are interested in both limit $\epsilon \to 0$ and $\delta \to 0$. We show that the scheme is AP for ϵ, but not for δ. Our numerical results confirm this statement. In particular, they show that the method is adequate for all range of ϵ, for fixed (but temporally resolved) δ, even including transitional ϵ where both small and large ϵ coexist.

The paper is organized as follows. In §2, we describe the time splitting spectral method that we shall use. In §3, the asymptotic limit is given for appropriate initial condition. In §4, we prove that the time splitting spectral method is asymptotic preserving in ϵ, and give an estimate on the numerical stability condition. Finally, numerical experiments are conducted in §5 to verify these conclusions. We make some ending remarks in §6.

2. The time splitting spectral method. The problem considered here can be expressed as

$$\delta\partial_t u_\epsilon + i\partial_t u_\epsilon = \Delta u_\epsilon + \frac{1}{\epsilon^2}(1-|u_\epsilon|^2)u_\epsilon, \quad \mathbf{x}\in\Omega \tag{2.1}$$

$$u_\epsilon(\mathbf{x}, t=0) = u_\epsilon^0(\mathbf{x}), \quad \mathbf{x}\in\Omega \tag{2.2}$$

In this paper, we only discuss the periodic boundary condition. The case of Dirichlet boundary condition is a straight forward extension ([2, 3]).

The time splitting method is described as follows. First solve

$$\begin{cases} \delta\partial_t \tilde{u}_\epsilon + i\partial_t \tilde{u}_\epsilon = \Delta \tilde{u}_\epsilon \\ \tilde{u}_\epsilon(0) = u_\epsilon^n \end{cases} \tag{2.3}$$

for one time step Δt, from $t = t^n = n\Delta t$ to an intermediate time t^*, to get $u_\epsilon^* = \tilde{u}_\epsilon(\Delta t)$. Then solve

$$\begin{cases} \delta\partial_t \breve{u}_\epsilon + i\partial_t \breve{u}_\epsilon = \frac{1}{\epsilon^2}(1-|\breve{u}_\epsilon|^2)\breve{u}_\epsilon \\ \breve{u}_\epsilon(0) = u_\epsilon^* \end{cases} \tag{2.4}$$

for one time step to get $u_\epsilon^{n+1} = \breve{u}_\epsilon(\Delta t)$.

The first step can be solved by the spectral method and integrate in time exactly. The second step is an ordinary differential equation that can easily been solved explicitly. Such a combination is referred to as the time splitting spectral method [4, 5].

The exact solution of (2.4), when $|u_\epsilon^*| \neq 0$ or 1, is:

$$\breve{u}_\epsilon(t) = \left(1 - \big(1 - \frac{1}{|u_\epsilon^*|^2}\big) e^{-\frac{2\delta}{\epsilon^2\delta^2+\epsilon^2} t}\right)^{-\frac{1}{2}(1-i/\delta)} \frac{u_\epsilon^*}{|u_\epsilon^*|^{1-i/\delta}}\,. \tag{2.5}$$

When $|u_\epsilon^*| = 0$ or 1, $\breve{u}_\epsilon(t)$ does not change with time.

In one dimension, consider the domain $\Omega = [a, b]$. Using a uniform spatial mesh size $\triangle x > 0$, with $\Delta x = (b_1 - a_1)/M$ for M an even positive integer. Define the grid points as

$$x_j := a + j\Delta x, \qquad j = 0, 1, \cdots, M.$$

Let U_j^n be the numerical approximation of $u_\epsilon(x_j, t^n)$, One can express the method explicitly as follows:

$$U_j^* = \frac{1}{M} \sum_{l=-M/2}^{M/2-1} e^{-\frac{k w_l^2}{(\delta+i)}} \hat{U}_l^n e^{i w_l (x_j - a)}, \quad j = 0, \cdots, M-1\,, \tag{2.6}$$

$$U_j^{n+1} = \left(1 - \big(1 - \frac{1}{|U_j^*|^2}\big) e^{-\frac{2\delta}{\epsilon^2\delta^2+\epsilon^2}\Delta t}\right)^{\frac{1}{2}(1-i/\delta)} \frac{U_j^*}{|U_j^*|^{1-i/\delta}}, \tag{2.7}$$

where $\hat{U}_l^n$, the Fourier coefficients of U_ϵ^n, is defined as

$$\hat{U}_l^n = \sum_{j=0}^{M-1} U_j^n e^{-i w_l (x_j - a)}\,, \qquad l = -M/2, \cdots, M/2 - 1\,, \tag{2.8}$$

with

$$w_l = \frac{2\pi l}{b-a}. \tag{2.9}$$

Here U_j^n is the approximation of $u_\epsilon(t_n, x_j)$.

The second order Strang splitting can be used here to get the second order accuracy in time. However, none of the conclusion in this paper will be altered.

3. The asymptotic limit. For the CGL equation (2.1), the physical observables are ρ_ϵ (the position density), $\mathbf{J}_\epsilon$ (the current density) and E_ϵ (the total energy), which can be computed from the wave function u_ϵ

$$\rho_\epsilon(\mathbf{x}, t) = |u_\epsilon(\mathbf{x}, t)|^2$$

$$\mathbf{J}_\epsilon(\mathbf{x}, t) = Im(\overline{u_\epsilon(\mathbf{x}, t)} \nabla u_\epsilon(\mathbf{x}, t))$$

$$\mathbb{E}_\epsilon(t) = \int_\Omega E_\epsilon(u_\epsilon) = \int_\Omega \frac{1}{2}|\nabla u_\epsilon|^2 + \frac{(1 - |u_\epsilon|^2)^2}{4\epsilon^2}$$

Let

$$p \wedge q = \mathrm{I}m(\overline{p}q) = \frac{1}{2i}(\overline{p}q - p\overline{q})$$

where p, q are two complex numbers. Multiplying both sides of (2.1) by $\overline{u}_\epsilon$ and taking the imaginary part lead to the conservation of mass

$$\partial_t |u_\epsilon|^2 = 2\mathrm{d}iv(u_\epsilon \wedge \nabla u_\epsilon) - 2\delta u_\epsilon \wedge \partial_t u_\epsilon. \tag{3.1}$$

Similarly, it is known ([18, 19]) that the conservation of linear momentum holds

$$\partial_t(u_\epsilon \wedge \nabla u_\epsilon) = 2\mathrm{d}iv(\nabla u_\epsilon \otimes \nabla u_\epsilon) - \nabla P_\epsilon - 2\delta \partial_t u_\epsilon \cdot \nabla u_\epsilon \tag{3.2}$$

with the pressure defined by

$$P_\epsilon = |\nabla u_\epsilon|^2 + u_\epsilon \cdot \triangle u_\epsilon - \frac{|u_\epsilon|^4 - 1}{2\epsilon^2} - \delta u_\epsilon \cdot \partial_t u_\epsilon. \tag{3.3}$$

In addition, the energy is dissipated as

$$\frac{d}{dt}\int_\Omega E_\epsilon(u_\epsilon)(t, \mathbf{x})d\mathbf{x} = -\delta \int_\Omega |\partial_t u_\epsilon|^2. \tag{3.4}$$

Note that, if $\delta = 0$, namely, for the NLS equation, this is the conservation of energy.

For an initial data u_ϵ^0 satisfying the periodic boundary condition, we make the following assumption

$$\mathbb{E}(u_\epsilon^0) = \int_\Omega \frac{1}{2}|\nabla u_\epsilon^0|^2 + \frac{(1 - |u_\epsilon^0|^2)^2}{4\epsilon^2} < C_0\,, \tag{3.5}$$

where C_0 is an ϵ-independent constant. It is known from Lemma 2.2 in [19] that under the above assumption, as $\epsilon \to 0$,

$$u_\epsilon^0 \to e^{i\phi(x)}, \tag{3.6}$$

for some $\phi(x)$. To be consistent with (3.6), in our numerical experiment later, we will use initial data of the following form

$$u_\epsilon^0 = e^{i\phi(x)} + \epsilon\varphi(\frac{x}{\epsilon})\,. \tag{3.7}$$

Now following [7] we discuss the limit equation of (2.1) as $\epsilon \to 0$. From the energy estimate (3.4), (3.6) is satisfied for all time $t > 0$. Assuming that $u_\epsilon \to u$ as $\epsilon \to 0$, then

$$|u| = 1\,. \tag{3.8}$$

Applying $|u| = 1$ in the conservation of mass (3.1), one arrives at the limit equation:

$$\delta u_t - \triangle u = u|\nabla u|^2. \tag{3.9}$$

More precisely, as is shown in Proposition 4 of [7], one has:

THEOREM 3.1. *Suppose δ does not depend on ϵ and the initial data given by (3.7). The solution to (2.1)(2.2) satisfies $u_\epsilon \to u$ in $\mathcal{C}((0,T), L^2)$ strongly and*

$L^\infty((0,T),H^1)$ weakly, where the limit u is the solution to (3.9) with initial data $u(0)=e^{i\phi(x)}$. Moreover, u satisfies the constraint (3.8) for all time.

If one writes $u=e^{i\theta}$ and assumes θ is smooth, then θ satisfies the heat equation

$$\delta\frac{\partial\theta}{\partial t}-\Delta\theta=0\,. \tag{3.10}$$

We note that this above analysis breaks down when there are vortices, since in this case, the perturbation to $e^{i\phi(x)}$ is not of order ϵ near the vortices. Nonetheless, we shall show numerically that the method still works in this case.

4. Asymptotic preserving and stability properties. In this section, we give heuristic arguments on the asymptotic preserving and stability properties of the TSSP presented in §2.

Let $\epsilon\to 0$. The first step (2.3) remains unchanged:

$$\begin{cases}(\delta+i)\partial_t\widetilde{u}=\Delta\widetilde{u}\,,\\ \widetilde{u}(0)=u_\epsilon^n\,,\end{cases} \tag{4.1}$$

while the second step (2.5) becomes

$$u^{n+1}=\frac{u^*}{|u^*|^{1-i/\delta}}\,. \tag{4.2}$$

From (4.2), it is obvious that

$$|u^{n+1}|=1,\qquad \arg(u^{n+1})=\frac{1}{\delta}\ln|u^{*n}|+\arg(u^{*n}), \tag{4.3}$$

where arg denotes the phase of u.

Now consider the first time step. Assuming that $|\widetilde{u}|$ does not go to zero at any point in one time step, then we can write $u=e^{A+i\theta}$ with A,θ being real functions depending on $\mathbf{x}$ and t. This assumption obviously requires that there are no vortices in the initial data. If so, then there are no vortices generated as time goes on [23]. Assume that A^n and θ^n are the real and imaginary parts of $\ln(u^n)$ respectively. Expressing the solution of (4.1) by $e^{\widetilde{A}+i\widetilde{\theta}}$ gives

$$\delta\widetilde{A}_t-\widetilde{\theta}_t=\nabla\widetilde{A}\cdot\nabla\widetilde{A}-\nabla\widetilde{\theta}\cdot\nabla\widetilde{\theta}+\triangle\widetilde{A}, \tag{4.4}$$

$$\delta\widetilde{\theta}_t+\widetilde{A}_t=2\nabla\widetilde{\theta}\cdot\nabla\widetilde{A}+\triangle\widetilde{\theta}\,, \tag{4.5}$$

with initial data A^n, θ^n. For this first step, after one time step, one gets A^* and θ^* at $t=t_*=t_n+\Delta t$. Note here t_* has a different meaning from t_{n+1}, which is important for our subsequent analysis.

Inserting these values into (4.3), then

$$A^{n+1}=0,\qquad \theta^{n+1}=\theta^*+\frac{1}{\delta}A^*. \tag{4.6}$$

If one solves the first step *exactly* in time, integrating (4.4) and (4.5) from t_n to t_*, one gets

$$A^*=A^n+\frac{1}{\delta^2+1}\int_{t_n}^{t_*}\Big(\delta(|\nabla\widetilde{A}|^2-|\nabla\widetilde{\theta}|^2+\Delta\widetilde{A})+(2\nabla\widetilde{\theta}\cdot\nabla\widetilde{A}+\Delta\widetilde{\theta})\Big)dt, \tag{4.7}$$

$$\theta^*=\theta^n+\frac{1}{\delta^2+1}\int_{t_n}^{t_*}\Big(-(|\nabla\widetilde{A}|^2-|\nabla\widetilde{\theta}|^2+\Delta\widetilde{A})+\delta(2\nabla\widetilde{\theta}\cdot\nabla\widetilde{A}+\Delta\widetilde{\theta})\Big)dt. \tag{4.8}$$

Note that from (4.6), when $\epsilon \to 0$, it implies that $A^n \to 0$ for all n. Thus

$$\theta^{n+1} = \theta^* + \frac{1}{\delta}A^* = \theta^n + \frac{1}{\delta}\int_{t_n}^{t_*} \big(2\nabla\widetilde{\theta}\cdot\nabla\widetilde{A} + \Delta\widetilde{\theta}\big)dt$$
$$\approx \theta^n + \frac{1}{\delta}\int_{t_n}^{t_*} \big(\Delta\widetilde{\theta}\big)dt\,. \tag{4.9}$$

Clearly, for fixed $\delta > 0$, (4.9) is consistent to the limit equation (3.10). Thus this splitting method is AP in ϵ for fixed δ.

Again, notice that the integral on the right hand side of (4.9) is over the time interval $[t_n, t_*]$. Since solution at t_* is used as the initial condition for the next step in the splitting method, (4.9) is effectively an *explicit* time discretization of the limit heat equation (3.10). When a spatial discretization is used in the first step of the time splitting method (4.1), the scheme, as $\epsilon \to 0$, is subject to the following stability condition

$$\Delta t \sim \delta(\Delta x)^2\,. \tag{4.10}$$

This is a rather severe stability condition for small δ, and becomes prohibitively expensive when $\delta \to 0$. Thus this method is *not* AP in δ.

In summary, the TSSP is AP in ϵ but not in δ.

5. Numerical examples. In our computations, the initial condition is always chosen as

$$u(x, t=0) = u_\epsilon^0(x) = e^{i\phi(x)} + \epsilon\varphi(\frac{x}{\epsilon})$$

with $\phi(x)$ independent of ϵ, real valued. We always choose the initial data with the correct periodicity. Define $\|u\|_2$ as the usual discrete l^2 norm on the interval (a, b), i.e.

$$\|u\|_2 = \sqrt{\frac{b-a}{M}\sum_{j=0}^{M-1}|u(x_j)|^2}\,.$$

In the following tables $e(\cdot)$ is the relative error between the exact solutions and the numerical ones. When U denotes the numerical solution while u denotes the 'exact' one computed with a very fine mesh, $e(U)$ is defined by

$$e(U) = \frac{\|U-u\|_2}{\|u\|_2}.$$

Most of the figures we present below contain four sub-figures. The top left shows the density $\rho_{\epsilon j} = |u_\epsilon(x_j)|^2$. The top right is the current $J_{\epsilon j}$ given by $\mathrm{Im}(\bar{u}_\epsilon(x_j)D_x^s u_\epsilon|_{x_j})$; the bottom left, the energy

$$E_{\epsilon j} = \frac{1}{2}\big|D_x^s u_\epsilon|_{x_j}\big|^2 + \frac{(1-|u_\epsilon(x_j)|^2)^2}{4\epsilon^2}$$

and the bottom right, the phase $S_{\epsilon j} = \arg(u_\epsilon(x_j))$. Here D_x^s is the spectral differential operators approximating ∂_x, which is defined by

$$D_x^s U|_{x=x_j} = -\frac{i}{M}\sum_{l=-M/2}^{M/2-1} w_l\hat{U}_l e^{i\nu_l(x_j-a)}, \tag{5.1}$$

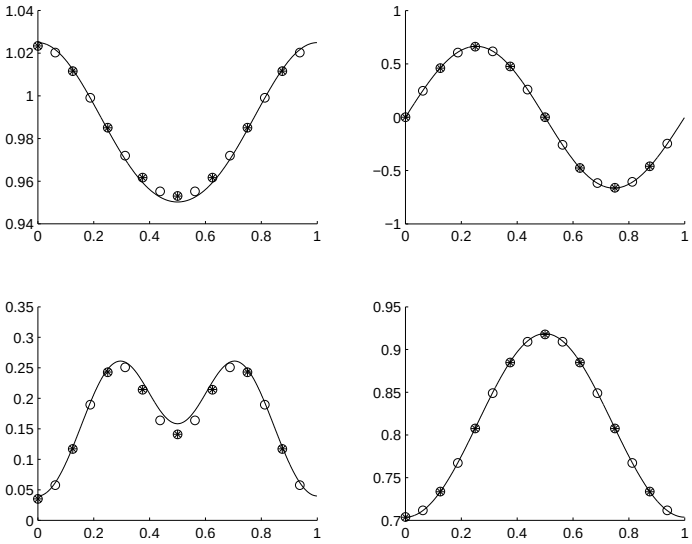

FIG. 5.1. *Example 1. Numerical solutions for* $\Delta x = 1/8$, $\Delta x = 1/16$ *and* $\Delta x = 1/1024$ *are presented by stars, circles and the solid lines respectively, with the same time step* $\Delta t = 1/400$. *Here the top left shows the density; the top right, the current; the bottom left, the energy and the bottom right, the phase.*

where $\hat{U}_l$, w_l are given in (2.8) (2.9).

The difference between the solution of the original CGL (2.1) (2.2) for a specific ϵ and the solution of the limit equation (3.8) (3.9) is denoted by $d(\cdot)$. Since the limit equation is valid when there are no vortices, we will use it only under such circumstances. Its solutions are calculated by using the spectral method for (3.10) and inserting the results into $u = e^{i\theta}$. Moreover, ρ, J, E, S for the limit u are defined the same as for u_ϵ.

Example 1: The initial condition in (5) is chosen with

$$\phi = 25(x(x-1))^2, \quad \varphi(x) = \sin(2\pi x), \quad \Omega = [0,1]\,.$$

First we check the convergence of the numerical method for fixed ϵ, δ as $\Delta x, \Delta t \to 0$ independently. For $\delta = 2$, $\epsilon = 1/8$, we compute the numerical solution with a very fine mesh, $\Delta x = 1/1024$ and a very small time step, $\Delta t = 1/128000$, as the reference 'exact' solution. The relative errors for different time and space steps are shown in Table 1. This shows that the scheme is spectrally convergent in space and first order convergent in time for all the qualities. Figure 1 shows the numerical results at $T = 0.1$. The quick convergence in space can be seen.

When ϵ, δ are small, the numerical scheme has a severe stability constraint as (4.10). When $\delta = O(1)$, the stability is unconditional. For instance, when $\delta = 3$, it is easy to check that whatever Δx and Δt are, the numerical results will not blow up. Figure 2 a) shows the numerical results at $T = 0.1$ when $\delta = 3$, $\epsilon = 0.001$, $\Delta x = 1/16$, $\Delta t = 1/400$. However when $\delta = 0.05$ with the same $\epsilon, \Delta x, \Delta t$ the numerical results grow unphysically due to the violation of the stability condition (4.10. Figure 2 b) plots the numerical solution at $T = 0.1$ with $\delta = 0.05, \epsilon = 0.001, \Delta x = 1/16, \Delta t = 1/400$. If Δt is chosen according to (4.10), then the numerical results give the correct solution.

Δx	Δt	$\|e(\rho_\epsilon)\|_2$	$\|e(J_\epsilon)\|_2$	$\|e(E_\epsilon)\|_2$	$\|e(S)\|_2$
1/8	1/128000	$2.36 * 10^{-5}$	$6.82 * 10^{-4}$	$1.45 * 10^{-3}$	$3.55 * 10^{-4}$
1/16	1/128000	$4.21 * 10^{-7}$	$6.04 * 10^{-5}$	$1.70 * 10^{-4}$	$9.96 * 10^{-5}$
1/32	1/128000	$1.01 * 10^{-7}$	$2.66 * 10^{-6}$	$5.86 * 10^{-6}$	$1.10 * 10^{-6}$
1/64	1/128000	$6.31 * 10^{-9}$	$1.65 * 10^{-7}$	$3.64 * 10^{-7}$	$6.81 * 10^{-8}$
1/64	1/400	$1.83 * 10^{-3}$	$5.10 * 10^{-3}$	$5.29 * 10^{-2}$	$6.90 * 10^{-4}$
1/64	1/800	$9.27 * 10^{-4}$	$2.54 * 10^{-3}$	$2.71 * 10^{-2}$	$3.54 * 10^{-4}$
1/64	1/1600	$4.64 * 10^{-4}$	$1.25 * 10^{-3}$	$1.36 * 10^{-2}$	$1.80 * 10^{-4}$

TABLE 5.1

Example 1. The relative errors for different time and space steps, with $\delta = 2$, $\epsilon = 1/8$.

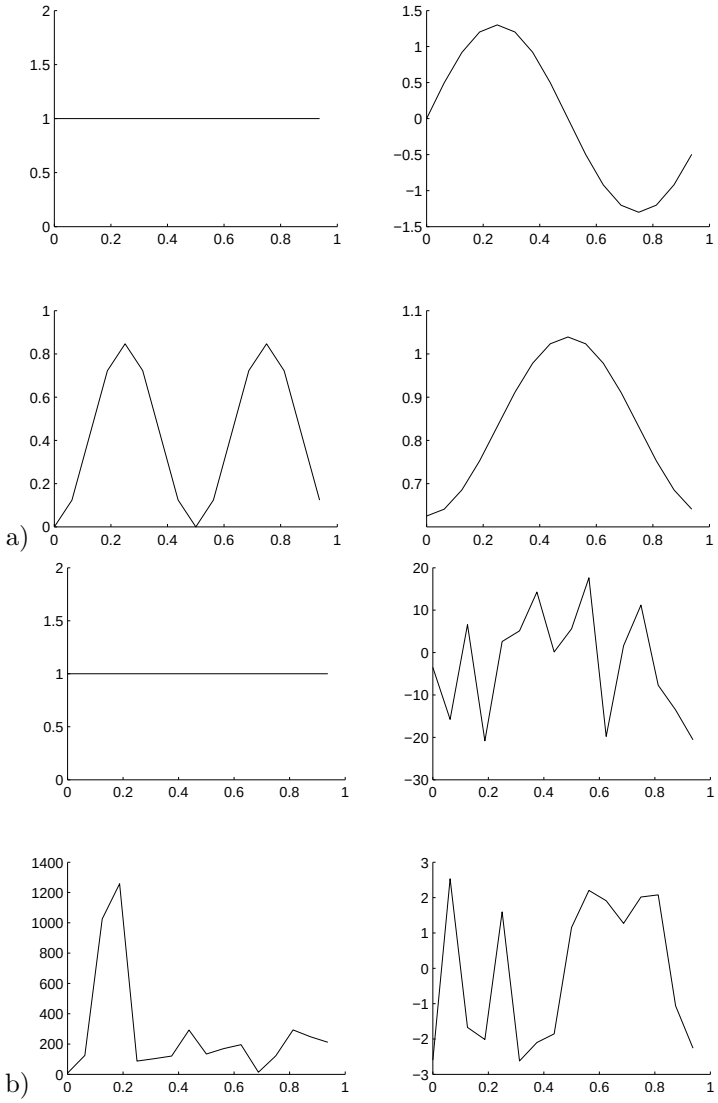

FIG. 5.2. *Numerical results at $T = 0.1$ with $\Delta x = 1/16$, $\Delta t = 1/400$. Top: a) $\delta = 3$; Bottom: b) $\delta = 0.05$. We can see that for δ small, the numerical result will blow up when the time step Δt is not small enough.*

Thirdly, we show the uniform convergence of TSSP with respect to ϵ when δ is fixed. This demonstrates the AP (in ϵ) property of the method. Two cases $\delta = 2$ and $\delta = 0.1$ are considered here. We compute the 'exact' numerical solution with a very fine mesh. For the $\delta = 2$ case, we use $\Delta x = 1/128$ and $\Delta t = 1/128000$, while for the $\delta = 0.1$ case, we take $\Delta x = 1/128$ and $\Delta t = 1/1638400$ for the stability reason.

Δx	Δt	ϵ	$\|e(\rho_\epsilon)\|_2$	$\|e(J_\epsilon)\|_2$	$\|e(E_\epsilon)\|_2$	$\|e(S)\|_2$
1/16	1/128000	1/2	$1.97 * 10^{-5}$	$3.48 * 10^{-5}$	$8.25 * 10^{-5}$	$1.30 * 10^{-5}$
1/16	1/128000	1/8	$4.21 * 10^{-6}$	$6.05 * 10^{-5}$	$1.70 * 10^{-4}$	$9.96 * 10^{-5}$
1/16	1/128000	1/32	$4.92 * 10^{-8}$	$3.14 * 10^{-5}$	$6.28 * 10^{-5}$	$1.91 * 10^{-5}$
1/16	1/128000	1/128	$3.17 * 10^{-9}$	$3.43 * 10^{-5}$	$6.87 * 10^{-5}$	$1.55 * 10^{-5}$
1/128	1/40	1/2	$1.01 * 10^{-2}$	$1.12 * 10^{-2}$	$4.69 * 10^{-2}$	$5.69 * 10^{-3}$
1/128	1/40	1/8	$1.44 * 10^{-3}$	$5.62 * 10^{-2}$	$3.41 * 10^{-1}$	$1.11 * 10^{-2}$
1/128	1/40	1/32	$1.49 * 10^{-3}$	$5.56 * 10^{-2}$	$1.09 * 10^{-1}$	$2.80 * 10^{-2}$
1/128	1/40	1/128	$8.80 * 10^{-5}$	$5.49 * 10^{-2}$	$1.01 * 10^{-1}$	$3.09 * 10^{-2}$

TABLE 5.2

Example 1. The relative error between the exact solutions and the numerical results at $T = 0.1$ when $\delta = 2$.

ϵ	$\|e(\rho_\epsilon)\|_2$	$\|e(J_\epsilon)\|_2$	$\|e(E_\epsilon)\|_2$	$\|e(S)\|_2$
1/2	$2.44 * 10^{-5}$	$2.58 * 10^{-4}$	$5.95 * 10^{-5}$	$4.10 * 10^{-5}$
1/8	$1.23 * 10^{-4}$	$4.19 * 10^{-3}$	$1.04 * 10^{-3}$	$1.34 * 10^{-3}$
1/32	$1.60 * 10^{-8}$	$9.59 * 10^{-3}$	$8.09 * 10^{-3}$	$3.43 * 10^{-5}$

TABLE 5.3

Example 1. The relative error between the exact solutions and the numerical results at $T = 0.1, \Delta x = 1/16, \Delta t = 1/25600$, when $\delta = 0.1$.

Figure 3 shows the numerical results at $T = 0.1$ for different values of ϵ and the limit equation. In this figure, if a type of line, e.g. '-.-.' or '...', is not visible from the figure, it indicates that the error is too small to be detected by eye. Clearly, when $\epsilon \to 0$, position density ρ_ϵ tends to 1.

For $\delta = 2$, Table 2 gives the relative error between the "exact" solutions and the numerical results with $\Delta x = 1/16, \Delta t = 1/128000$ and $\Delta x = 1/128, \Delta t = 1/40$ for different ϵ. It is easy to see that the error is almost independent of ϵ. When $\delta = 0.1$, the relative errors between the "exact" solutions and the numerical ones with $\Delta x = 1/16, \Delta t = 1/25600$ for different ϵ are presented in Table 3. Both tables demonstrate the error is basically independent of ϵ for fixed δ. This verifies the AP (in ϵ) property of the method.

Finally, the convergence of the solution of CGL when $\epsilon \to 0$ to the solution of the limit problem is investigated, with time and space steps fixed and small (compared to ϵ and δ). The difference between the "exact" solution of the CGL to the limit equation (3.9) as $\epsilon \to 0$ is presented in Table 4 and Table 5 for $\delta = 2, 0.1$ respectively. Here the reference 'exact' solution of the limit equation is obtained by the spectral method with $\Delta x = 1/128$. The results for different ϵ and the limit equation are presented in Figure 3, which confirm that the limit equation is a good approximation of CGL for ϵ small. We can see from Table 4 that the convergence rate of CGL to the limit heat equation when $\epsilon \to 0$ is about ϵ^2. In Table 5 "$-$" stands for machine precision. The error in this Table is much smaller, since the solution, for such a small δ, basically

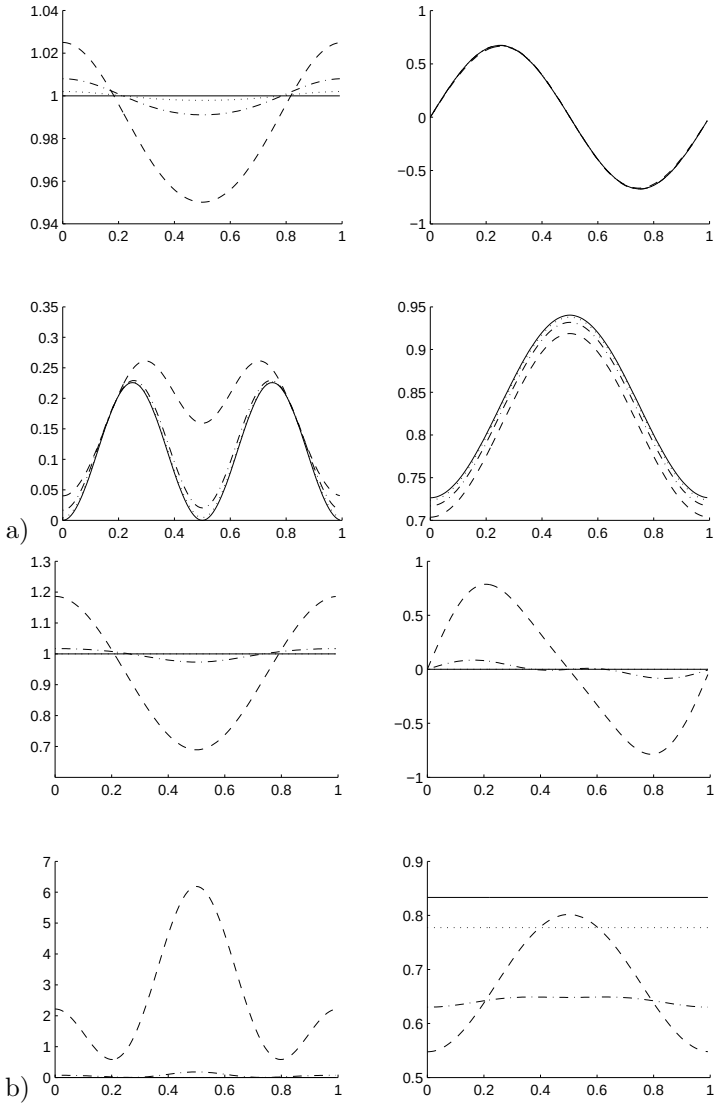

FIG. 5.3. *Example 1. Exact solution of the limit equation by solid line, exact solution of the CGL for* $\epsilon = 1/8$ *by dashed line,* $\epsilon = 1/16$ *by dashdotted line and* $\epsilon = 1/32$ *by dotted line. Because some of the curves are superimposed, In some figures, see one curve is seen. a)* $\delta = 2$, $T = 0.1$*; b)* $\delta = 0.1$, $T = 0.1$.

reached the steady state already at the time of the output.

Example 2: Consider a two dimensional example, with initial condition (5) given by taken as

$$\delta = 1, \quad \phi(x,y) = 100(x^2 - x)^2(y^2 - y)^2, \quad \varphi(x,y) = \frac{1}{4}(\sin(2\pi x) + i * \sin(2\pi y)) .$$

ϵ	$\|d(\rho_\epsilon)\|_2$	$\|d(J_\epsilon)\|_2$	$\|d(E_\epsilon)\|_2$	$\|d(S)\|_2$
1/8	$3.40 * 10^{-1}$	$8.05 * 10^{-2}$	$9.32 * 10^{-1}$	$2.69 * 10^{-1}$
1/16	$6.93 * 10^{-2}$	$2.63 * 10^{-2}$	$1.42 * 10^{-1}$	$1.06 * 10^{-1}$
1/32	$1.69 * 10^{-2}$	$1.03 * 10^{-2}$	$3.46 * 10^{-2}$	$3.02 * 10^{-2}$
1/64	$4.15 * 10^{-3}$	$2.86 * 10^{-3}$	$8.47 * 10^{-3}$	$7.83 * 10^{-3}$
1/128	$9.96 * 10^{-4}$	$6.99 * 10^{-4}$	$1.96 * 10^{-3}$	$1.98 * 10^{-3}$

TABLE 5.4

Example 1. The difference between the solution of the original CGL for a specific ϵ and the solution of the limit equation when $\delta = 2$.

ϵ	$\|d(\rho_\epsilon)\|_2$	$\|d(J_\epsilon)\|_2$	$\|d(E_\epsilon)\|_2$	$\|d(S)\|_2$
1/8	2.10	6.09	35.3	2.05
1/16	$1.76 * 10^{-1}$	$5.65 * 10^{-1}$	$9.35 * 10^{-1}$	2.16
1/32	$4.73 * 10^{-5}$	$6.25 * 10^{-4}$	$2.58 * 10^{-7}$	$6.32 * 10^{-1}$
1/64	–	–	–	$1.63 * 10^{-1}$
1/128	–	–	–	$4.10 * 10^{-2}$

TABLE 5.5

Example 1. The difference between the solution of the original CGL for a specific ϵ and the solution of the limit equation when $\delta = 0.1$. The "–" stand for machine precision.

We compute the solution on the rectangle $[0, 1] \times [0, 1]$ with periodic boundary conditions. For two dimension, the current is a vector. In the tables and figures presented in this example, we just plot or analyze the component in the x direction J_1. Figure 4 shows the "exact" result at $T = 0.1$ for $\epsilon = 1, 1/128$ computed with $\Delta x = 1/128$ and $\Delta t = 1/128000$. This solution is already quite close to the exact solution, because the spectral method is spectrally accurate in space. Table 6 gives the relative errors between the numerical results with $\Delta x = 1/16, \Delta t = 1/640$ and the "exact" solutions for different values of ϵ, showing the error independent of ϵ.

ϵ	$\|e(\rho_\epsilon)\|_2$	$\|e(J_\epsilon)\|_2$	$\|e(E_\epsilon)\|_2$	$\|e(S)\|_2$
1/16	$4.87 * 10^{-5}$	$2.07 * 10^{-2}$	$1.47 * 10^{-1}$	$3.64 * 10^{-4}$
1/32	$4.38 * 10^{-5}$	$2.83 * 10^{-2}$	$1.19 * 10^{-1}$	$7.99 * 10^{-4}$
1/64	$1.84 * 10^{-5}$	$4.84 * 10^{-2}$	$1.07 * 10^{-1}$	$1.79 * 10^{-3}$
1/128	$4.99 * 10^{-6}$	$5.90 * 10^{-2}$	$1.17 * 10^{-1}$	$2.32 * 10^{-3}$

TABLE 5.6

Example 2. The relative errors between the exact solutions and the numerical solutions computed with $\Delta x = 1/16, \Delta t = 1/640$ for different ϵ.

Figure 5 displays the solution of the limit equation at $T = 0.1$ calculated by a spectral method with $\Delta x = 1/128$ and exact integration in time. The differences of the limit solution to the exact solutions of CGL for different values of ϵ are given Table 7. Now the convergence rate in two dimensional case seems to be of order ϵ.

Example 3: In this example we consider a general form of the CGL given by

$$\delta \partial_t u_\epsilon + i \partial_t u_\epsilon = \triangle u_\epsilon + \frac{1}{\epsilon^2}(V(x) - |u_\epsilon|^2) u_\epsilon, \quad x \in \Omega. \tag{5.2}$$

ϵ	$\|d(n)\|_2$	$\|d(J_1)\|_2$	$\|d(E)\|_2$	$\|d(S)\|_2$
1/32	$7.32 * 10^{-5}$	$7.83 * 10^{-4}$	$1.09 * 10^{-5}$	$3.44 * 10^{-4}$
1/64	$1.87 * 10^{-5}$	$3.21 * 10^{-4}$	$3.77 * 10^{-6}$	$1.10 * 10^{-4}$
1/128	$5.12 * 10^{-6}$	$1.50 * 10^{-4}$	$1.58 * 10^{-6}$	$4.25 * 10^{-5}$

TABLE 5.7

Example 2. The difference between the solution of the original CGL for a specific ϵ and the solution of the limit equation.

Here $V(x)$ is a given positive-valued external potential satisfying $V(x) \to 1$ when $x \to \partial\Omega$. We can use the same TSSP to deal with this problem. As is mentioned in [3], the exact solution of the second step becomes

$$u_\epsilon(t) = \left(\frac{V(x)}{|u_\epsilon(0)|^2 - \big(|u_\epsilon(0)|^2 - V(x)\big) e^{-\frac{2\delta}{\epsilon^2\delta^2+\epsilon^2} V(x) t}} \right)^{\frac{1}{2}(1-i/\delta)} u_\epsilon(0), \tag{5.3}$$

when $V(x) \neq 0$. Using the same process as in §3, it is easy to check that as $\epsilon \to 0$, the limit of (5.2) is

$$\mathrm{d}iv(u \wedge \nabla u) - \delta u \wedge \partial_t u = 0, \qquad |u| = \sqrt{V(x)} \quad \text{a.e.}, \qquad u(0) = u^0.$$

Write $u^n = \sqrt{V(x)} e^{i\theta(x)}$, the above equation is equivalent to

$$\delta\theta_t = \triangle\theta + \nabla\theta \cdot \nabla \ln V. \tag{5.4}$$

Furthermore, the limit scheme of time splitting is

$$(\delta + i)\partial_t \widetilde{u} = \Delta\widetilde{u}, \qquad u^{n+1} = u^* \left(\frac{V(x)}{|u^*|^2} \right)^{\frac{1}{2}(1-i/\delta)}.$$

The limit of the second step written in the A^*, θ^* form as in (4.6) is

$$A^{n+1} = \frac{1}{2} \ln V(x), \qquad \theta^{n+1} = \theta^* + \frac{1}{\delta} A^* - \frac{1}{2\delta} \ln V(x).$$

A similar argument as in the case of $V(x) = 1$ implies that this scheme is AP when $\epsilon \to 0$, with $A^n \to 1/2 \ln V(x)$.

For the numerical example, we take

$$\delta = 2, \qquad \epsilon = e^{-4}, \qquad \Omega = [-2, 2], \tag{5.5}$$

and

$$V(x) = \begin{cases} 1, & x \in [-2, -1.5] \\ e^{6x^3+18x^2+13.5x}, & x \in [-1.5, -0.5] \\ e^{-3}, & x \in [-0.5, 0.5] \\ e^{-6x^3+18x^2-13.5x}, & x \in [0.5, 1.5] \\ 1 & x \in [1.5, 2] \end{cases}, \tag{5.6}$$

Since the energy is defined by

$$E_\epsilon(u_\epsilon) = \frac{1}{2}|\nabla u_\epsilon|^2 + \frac{(V(x) - |u_\epsilon|^2)^2}{4\epsilon^2}.$$

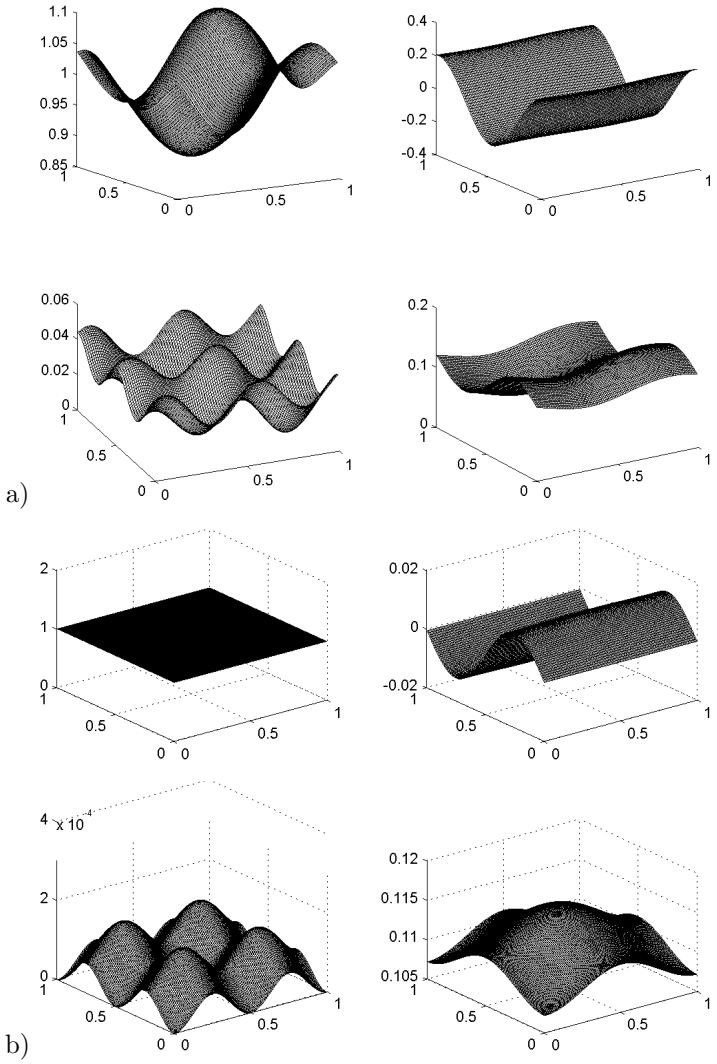

FIG. 5.4. *Example 2. 'Exact' solutions at $T = 0.1$ for different values of ϵ are presented. Here the top left shows the density; the top right, the current; the bottom left, the energy and the bottom right, the phase. a): $\epsilon = 1$; b): $\epsilon = 1/128$.*

We to keep the energy it when $\epsilon \to 0$, the initial data should be chosen as $\sqrt{V(x)}e^{i\phi(x)}$. Here $\phi(x) = 0.2(x+2)^2(x-2)^2$. The "exact" solution is given numerically with very small time and space steps $\Delta x = 1/1000, \Delta t = 1/30000$. Figure 6 a) shows $V(x)$ and Figure 6 b) demonstrates the AP property of this scheme.

Example 4: Assume V(x) changes from $O(1)$ in one region to $O(\epsilon^2)$ values in another region. The scale ϵ is related to the size of $V(x)$ and it can be seen that the case $V(x) = O(\epsilon^2)$ would require a change of ϵ to a new scale of order 1. Therefore, this example involves the transition regime between a region when ϵ is small to a region

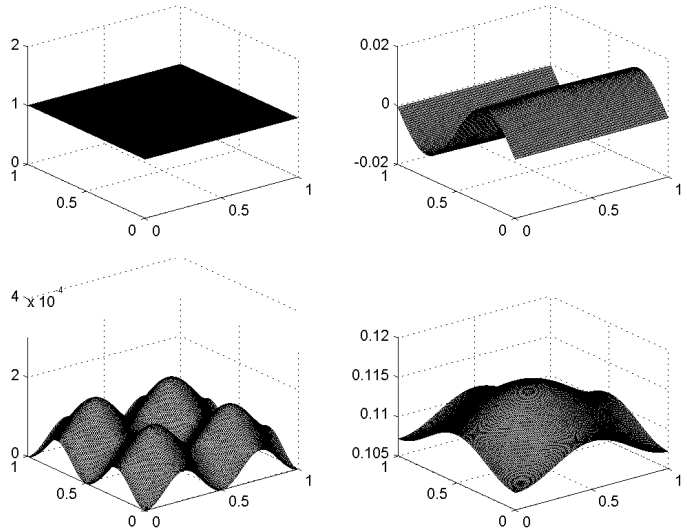

FIG. 5.5. *Example 2. The solution of the limit equation at $T = 0.1$. Here the top left shows the density; the top right, the current; the bottom left, the energy and the bottom right, the phase.*

where it is of order 1. We know that the scheme performs well in both the $\epsilon = O(1)$ and the $\epsilon \ll 1$ regimes separately. We now want to investigate how the scheme performs in the transition region between $\epsilon = O(1)$ region to the $\epsilon \ll 1$ region. Use the same parameter as in (5.5) and take

$$V(x) = \begin{cases} 1, & x \in [-2, -1.5] \\ e^{16x^3+48x^2+36x}, & x \in [-1.5, -0.5] \\ e^{-8}, & x \in [-0.5, 0.5] \\ e^{-16x^3+48x^2-36x}, & x \in [0.5, 1.5] \\ 1 & x \in [1.5, 2] \end{cases}$$

$u_\epsilon^0(x) = \sqrt{V(x)}e^{i\phi(x)}$, $\phi(x) = 0.5(x+2)^2(x-2)^2$. This can be regarded as a transition between an $\epsilon = O(1)$ region (the exterior left and right interval) and an $\epsilon \ll 1$ region (the middle interval). The transition regions are the two intermediate intervals. The numerical results are shown in Figure 7. One can see that the scheme also performs well in this transition problem.

In fact this transitional case can be viewed as a special form of the standard and asymptotic regimes coexisting case. Inserting

$$u_\epsilon = \sqrt{V(x)}\tilde{u} \tag{5.7}$$

into (5.2) and using the fact that

$$\triangle \ln V(x) = \nabla \cdot \frac{\nabla V(x)}{V(x)} = \frac{\triangle V(x)}{V(x)} - |\nabla \ln V(x)|^2,$$

one gets

$$(\delta + i)\partial_t \tilde{u} = \triangle \ln V(x)\tilde{u} + |\nabla \ln V(x)|^2\tilde{u} + \nabla \ln V(x) \cdot \nabla \tilde{u} + \triangle \tilde{u} + V(x)\frac{1 - |\tilde{u}|^2}{\epsilon^2}\tilde{u}\,. \tag{5.8}$$

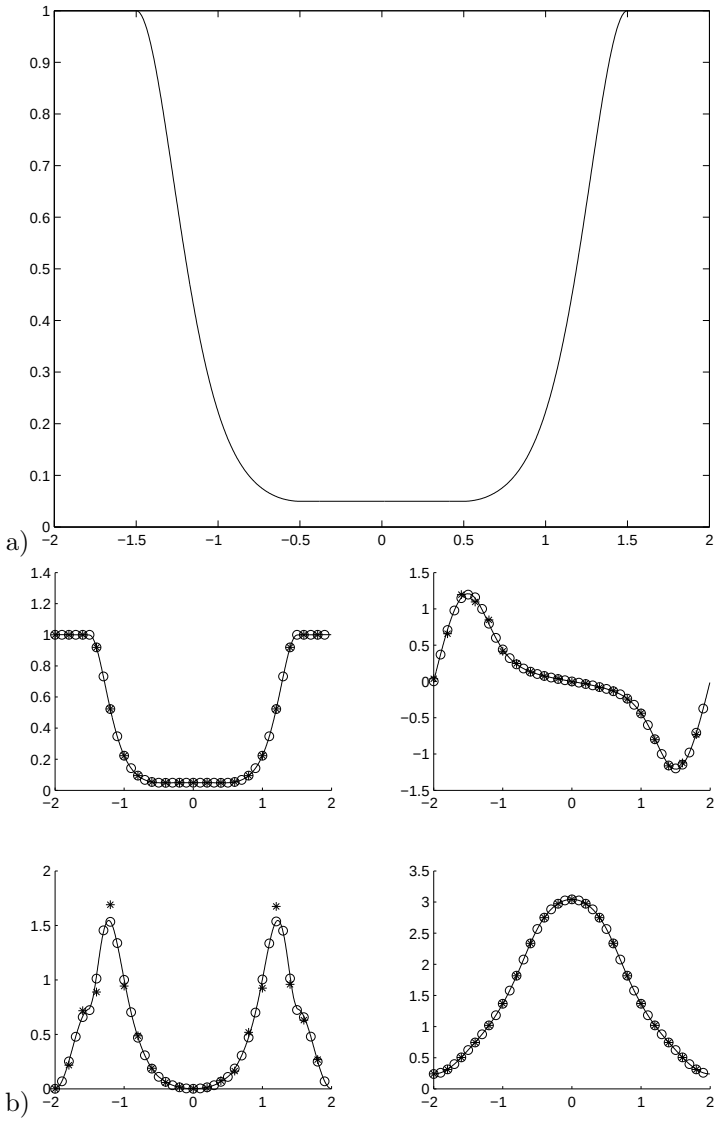

FIG. 5.6. *Example 3. Top: potential V as shown in (5.6); Bottom: Exact solution at $T = 0.1$ (solid line), the numerical results for $\Delta x = 1/5, \Delta t = 1/200$ (stars) and $\Delta x = 1/20, \Delta t = 1/400$ (circles).*

in the above example, in the middle interval [-0.5,0.5], $V(x) = \epsilon^2$, so the above equation becomes

$$(\delta + i)\partial_t \tilde{u} = \triangle \tilde{u} + (1 - |\tilde{u}|^2)\tilde{u},$$

which is the CGL in the standard regime. In the interval $[-2, -1.5] \cup [1.5, 2]$, $V(x) = 1$, so one finds CGL in the asymptotic regime. Figure 8 gives the numerical result of $\tilde{u}$ which is obtained from applying the transform to u. This result confirms again the applicability of this scheme to a situation where the standard and asymptotic regimes coexist.

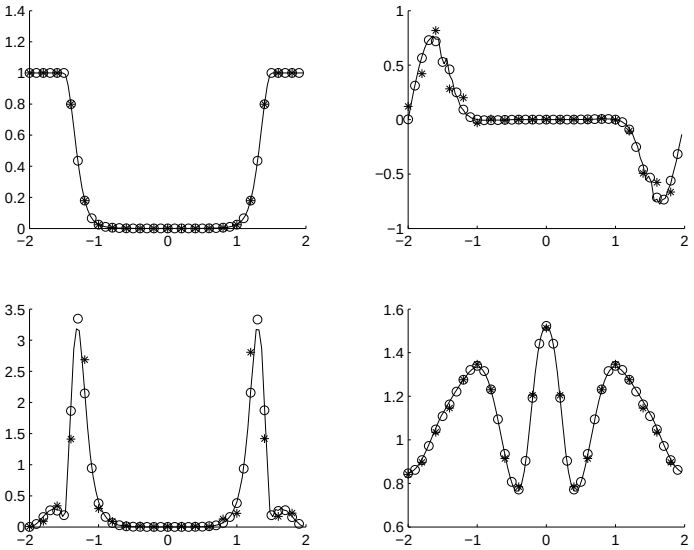

FIG. 5.7. *Example 4. The exact solution of u at $T = 0.1$ (solid line) and the numerical results for $\Delta x = 1/5, \Delta t = 1/200$ (stars) and $\Delta x = 1/10, \Delta t = 1/400$ (circles). Here $\epsilon = 10^{-4}$*

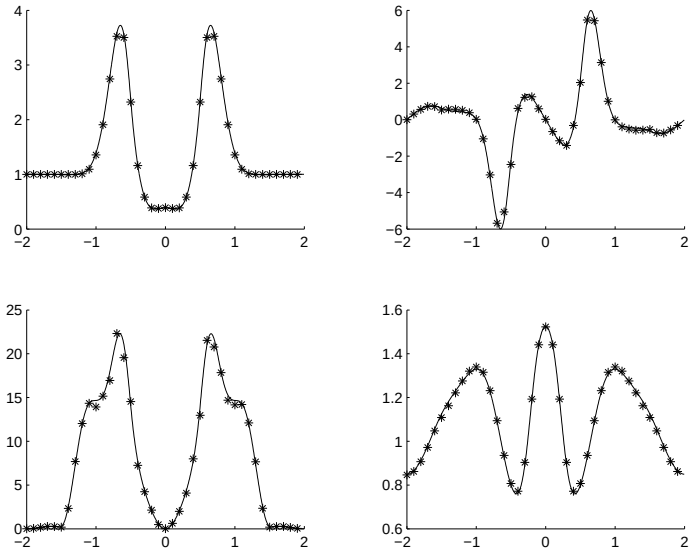

FIG. 5.8. *Example 4. The exact solution of (5.8) at $T = 0.1$ (solid line) and the numerical results for $\Delta x = 1/10, \Delta t = 1/400$ (stars), which are obtained from applying the transform (5.7) to u.*

Example 5: The rich dynamics of quantized vortices governed by the CGL is an interesting problem studied in many application fields. Vortices are points where $|u_\epsilon|$ becomes zero and the phase of u_ϵ or $u_\epsilon/|u_\epsilon|$ has singularities. In the superfluid theory, these points are the locations of the regular fluid, which are surrounded by

the superfluid. The degree of a vortex is defined by

$$\deg u_\epsilon = \frac{1}{2\pi}\int_{|x-x_0|=R} d(\arg u_\epsilon),$$

with $R < R_0$, where x_0 is the location of the vortex and R_0 is the radius of the large disk which contains no vortex other than x_0. The motion of degree one vortices as ϵ goes to zeros is studied analytically [23, 18, 19], and it is shown formally that the reduced dynamics law for CGL is a combination of the reduced dynamics law for GLE and NLS. Some numerical results are given in [2, 3]. For the periodic case, we assume that the sum of degrees $\sum_{j=1}^{n} n_j = 0$. Here n is the number of vortices and n_j is the degree of the jth vortex. This condition is needed in the periodic case in order to maintain the boundary condition. Indeed, it can easily be shown in the periodic case that the degree related to the boundary is necessarily 0.

In this example, we test if our method can be used when the initial condition contains two opposite vortices. The parameters are

$$\delta = 1, \qquad \epsilon = 0.1, \qquad \Omega = [-1,1]\times[-1,1]$$

and the initial condition is taken as

$$u_\epsilon^0(0,0.5) = 0; \qquad u_\epsilon^0(0,-0.5) = 0; \qquad u_\epsilon^0 = \rho(x)e^{i\phi(x)}, \quad \text{when} \quad |u_\epsilon| \neq 0$$

where

$$\rho = \begin{cases} 1 - e^{1-\frac{\epsilon^2}{\epsilon^2 - x^2 - (y-0.5)^2}}, & x^2 + (y-0.5)^2 < \epsilon^2 \\ 1 - e^{1-\frac{\epsilon^2}{\epsilon^2 - x^2 - (y+0.5)^2}} & x^2 + (y+0.5)^2 < \epsilon^2 \\ 1 & \text{elsewhere} \end{cases}$$

$$\phi = \begin{cases} \arg(x+i(y+0.5)) - \arg(x+i(y-0.5)) & x^2+y^2 < 0.75^2 \\ \left(\arg(x+i(y-0.5)) - \arg(x+i(y-0.5))\right) & \\ \quad \times\left(e^{-\frac{(\sqrt{x^2+y^2}-0.75)^2}{0.25^2-(\sqrt{x^2+y^2}-0.75)^2}}\right) & 0.75^2 \le x^2+y^2 < 1 \\ 0 & \text{elsewhere.} \end{cases}$$

The initial condition has two vortices at (0,0.5) and (0,-0.5) and satisfies the periodic boundary condition. Figure 9 shows the initial condition and Figure 10 a) and b) display the numerical results at time $T = 0.2$ and $T = 0.5$ respectively with $\Delta x = 1/100, \Delta t = 1/2000$. In order to find the location of the vortices, in Figure 11 a), b), we depict the contour lines of the phase for $T = 0$ and $T = 0.2$ respectively. It is easy to find that the vortices attract each other, collide and disappear as time goes on. This is consistent with the analytical results [23] and numerical ones [2, 3]. The time and space steps we use for these results resolve ϵ and ϵ^2 respectively. We can use even finer meshes to show the convergence of the numerical method. If we use coarser meshes such as $\Delta x = 1/10, \Delta t = 1/100$, the numerical results are given in Figure 12 a) and b). We can see that the structure of the solution can be captured with unresolved mesh.

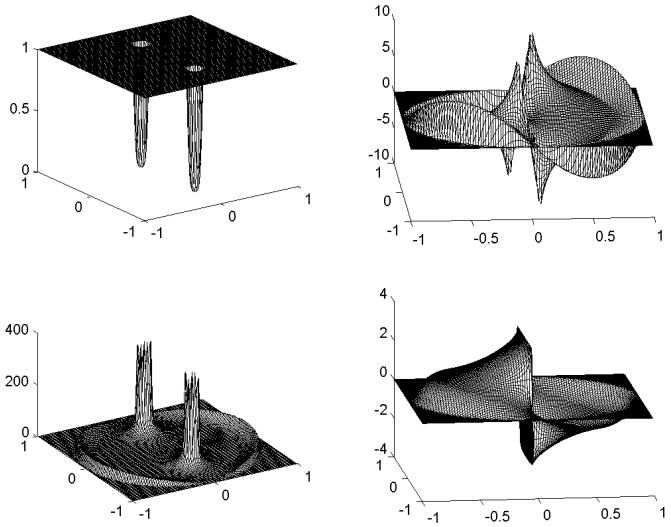

FIG. 5.9. *The initial condition for example 5. Here the top left shows the density; the top right, the current; the bottom left, the energy and the bottom right, the phase.*

6. Conclusion. The time splitting spectral method (TSSP) for the CGL equation (2.1) is investigated in this paper. We heuristically argue that the method is asymptotic preserving in the large space and time limit, but not in the nonlinear Schrödinger (NLS) limit. Moreover, the method suffers a severe numerical stability constrain in the NLS regime. Our numerical experiments confirm this conclusion.

In the large space and time limit, the method can capture the correct macroscopic behavior without numerical resolving the small scales. This was shown by numerical examples in both one and two space dimensions, including transitional regime and vortices.

In the future, we will investigate possible numerical schemes that are also AP in δ.

REFERENCES

[1] I. S. ARANSON AND L. KRAMER, *The world of the complex Ginzburg –Landau equation*, Reviews of Modern Physics, 74(1)(2002), pp. 100–138

[2] W. BAO, Q. DU AND Y. ZHANG, *The Dynamics and Interaction of Quantized Vortices in Ginzburg-Landau-Schroedinger equations*, SIAM J. Appl. Math., 67(6)(2007.),pp. 1740–1775.

[3] W. BAO, Q. DU AND Y. ZHANG, *Numerical simulation of vortex dynamics in Ginzburg-Landau-Schrödinger equation*, Eur. J. Appl. Math., 18(2007) pp. 607–630.

[4] W. BAO, S. JIN AND P. A. MARKOWICH, *On time splitting spectral approximations for the Schrödinger equation in the semiclassical regime*, J. Comput. Phys., 175 (2002), pp. 487–524.

[5] W. BAO, S. JIN AND P. A. MARKOWICH, *Numerical study of time-splitting spectral discretizations of nonlinear Schrödinger equations in the semi-classical regimes*, SIAM J. Sci. Comp., 25 (2003), pp. 27–64.

[6] C. BESSE, B. BIDÉGARAY AND S. DESCOMBES, *Order estimates in time of splitting methods for the nonlinear Schrödinger equation*, SIAM J. Numer. Anal. 40 (2002), pp. 26–40.

[7] T. COLIN AND A. SOYEUR, *Some singular limits for evolutionary Ginzburg-Landau equations*, Asymptotic Analysis, 13 (1996), pp. 361–372.

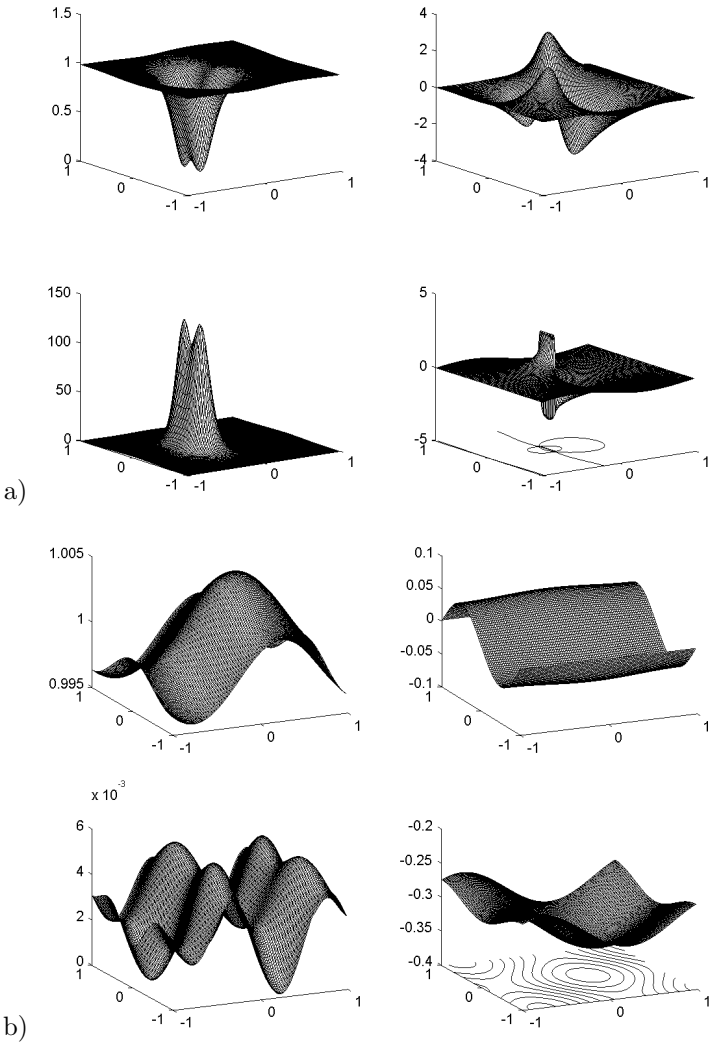

FIG. 5.10. *Example 5. The numerical results of density, current, energy and phase, from top left to bottom right, given by* $\Delta x = 1/100, \Delta t = 1/2000$ *at a)* $T = 0.2$ *and b)* $T = 0.5$ *respectively.*

[8] P. CRISPEL, P. DEGOND AND MH. VIGNAL, *An asymptotic preserving scheme for the two-fluid Euler-Poisson model in the quasineutral limit*, J. Comput. Phys.,223(2007),pp. 208-234.

[9] M. C. CROSS AND P. C. HOHENBERG, *Pattern formation outside of equilibrium*, Rev. Mod. Phys., 65(1993), pp. 851C-1112.

[10] G. DANGELMAYR AND L. KRAMER, *Mathematical approaches to patten formation, in Evolution of Spontaneous Structures in Dissipative Continuous Systems*, F. H. Busse and S. D. *Müller* ed., Springer, NewYork, 1998, pp. 1.

[11] R. C. DIPRIMA, W. ECKHAUS, AND L. A. SEGEL, *Non-linear wave number interaction in near critical two-dimensional flows*, J. Fluid Mech., 49(1971), pp. 705–744

[12] A. DOELMAN, *finite-dimensional models of the Ginzburg-Landau equation*, Nonlinearity, 4 (1991), pp. 231–150.

[13] F. GOLSE, S. JIN AND C.D. LEVERMORE, *The Convergence of Numerical Transfer Schemes in Diffusive Regimes I: The Discrete-Ordinate Method*, SIAM J. Num. Anal. 36 (1999), pp. 1333–1369.

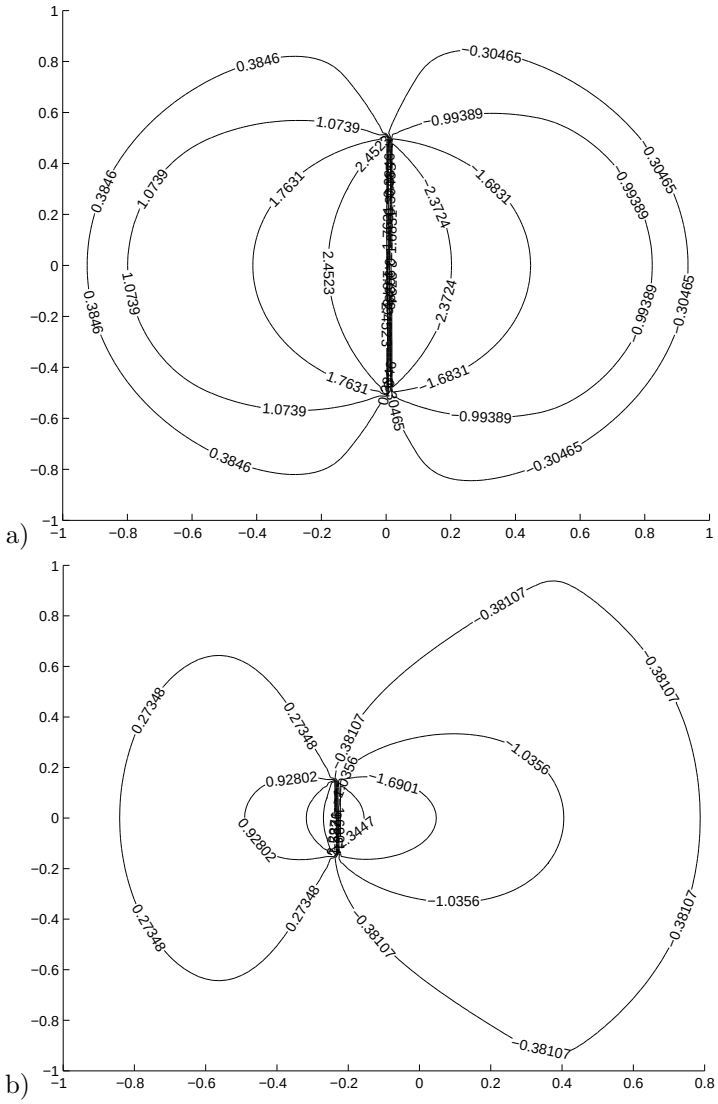

FIG. 5.11. *Example 5. Contour lines of the phase of the initial condition and numerical results at* $T = 0.2$. *Top:* $T = 0$*; Bottom:* $T = 0.2$

[14] Z. HUANG, S. JIN, P.A. MARKOWICH, C. SPARBER AND C. ZHENG, *A time-splitting spectral scheme for the Maxwell-Dirac system*, J. Comp. Phys. 208 (2005), pp. 761–789.

[15] S. JIN, *Efficient Asymptotic-Preserving (AP) Schemes for Some Multiscale Kinetic Equations*, SIAM J. Sci. Comp., 21 (1999), pp. 441–454.

[16] S. JIN, P.A. MARKOWICH AND C. ZHENG, *Numerical simulation of a generalized Zakharov system*, J. Comp. Phys. 201(2004), pp. 376-395, .

[17] C. D. LEVERMORE AND M. OLIVER, *The complex Ginzburg-Landau equation as a model problem*, Dynamical systems and probabilistic methods in PDEs (Berkeley, CA, 1994), pp. 141–190, Lectures in Appl. Math., 31, Amer. Math. Soc., Providence, RI, 1996.

[18] F. H. LIN, *Complex Ginzburg-Landau equaitons and dynamics of vortices, filaments, and codimension-2 submanifolds*, Comm. Pure Appl. Math., LI (1998), pp. 0385–0441.

[19] F. H. LIN AND J. X. XIN, *On the incompressible fluid limit and the vortex motion law of the nonlinear Schrödinger equation*, Commun. Math. Phys. 200 (1999), pp. 249–274.

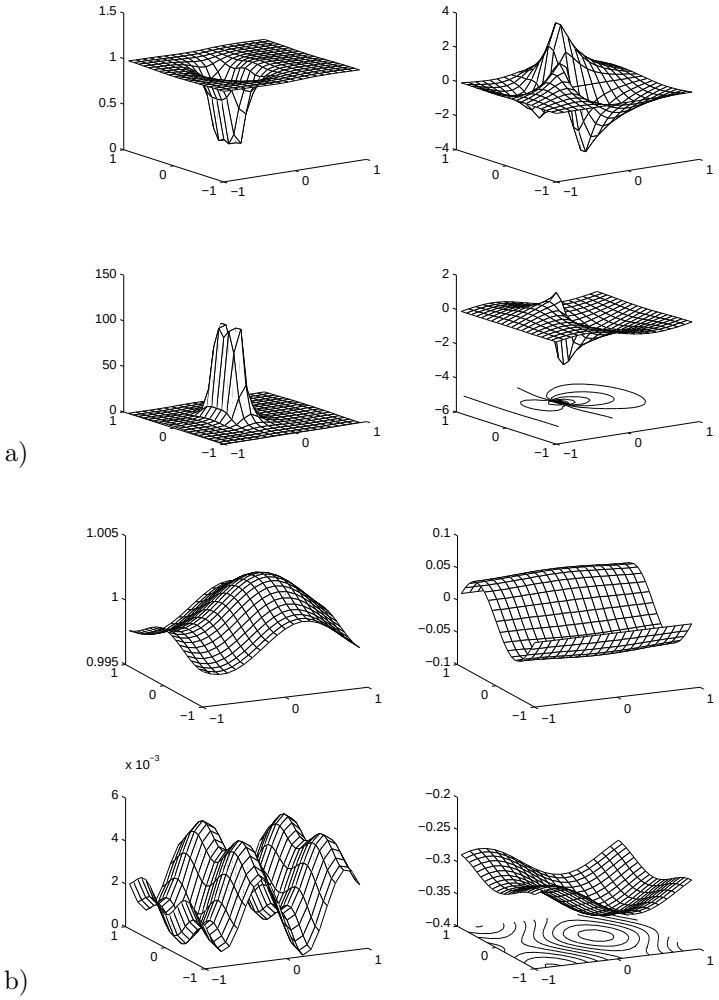

FIG. 5.12. *Example 5. The numerical results density, current, energy and phase, from top left to bottom right, given by* $\Delta x = 1/10, \Delta t = 1/100$ *at a)* $T = 0.2$ *and b)* $T = 0.5$.

[20] G.J. LORD, *Attractors and inertial manifolds for finite-difference approximations of the complex Ginzburg-Landau equation*, SIAM J. Num. Anal. 34 (1997), pp. 1483–1512.

[21] G.J. LORD AND A.M. STUART, *Discrete Gevrey regularity, attractors and upper-semicontinuity for a finite difference approximation to the Ginzburg-Landau equation*, Num. Funct. Anal. Optim. 16(1995), pp. 1003–1047.

[22] C. LUBICH, *On splitting methods for Schrödinger-Poisson and cubic nonlinear Schrödinger equations*, Math. Comp., to appear.

[23] J. C. NEU, *Vortices in complex scalar fields*, Physica D, 43 (1990), pp. 407–420

[24] A. C. NEWELL AND J. A. WHITEHEAD, *Review of the finite bandwidth concept*, in Proceedings of the International Union of Theoretical and Applied mechanics, Symposium on Instability of Continuous Systems, 1969, H. Leipholz ed., Springer-Verlag, Berlin 1971, pp. 279–303

[25] A. C. NEWELL AND J. A. WHITEHEAD, *Finite bandwidth, finite amplitude convection*, J. Fluid Mech., 38(1969), pp. 279–303

[26] D. PATHRIA AND J. L. MORRIS, *Pseudo-spectral solution of nonlinear Schrödinger equation*, J. Comput. Phys., 87(1990), pp. 108

[27] L.A. Segel, *Distant side-walls cause slow amplitude modulation of celluar convection*, J. Fluid Mech., 38(1969), pp. 203–224
[28] K. Stewarton and J. T. Stuart, *A nonlinear instability theory for a wave system in plane poiseuille flow*, J. Fluid Mech., 48(1971), pp. 529–549
[29] P. Takác and A. Jüngel, *A nonstiff Euler discretization of the complex Ginzburg-Landau equation in one space dimension*, SIAM J. Num. Anal. 38 (2000), pp. 292–328.
[30] A. Torcini, H. Frauenkron and P. Grassberger, *Studies of phase turbulence in the one-dimesional complex Ginzburg-Landau equation*, Phys. Rev., 55(5)(1997).